International Journal of
Molecular Sciences

MDPI

Article

Adsorption and Sensing Performance of Pt(1-3)-Modified $TiSe_2$ for Dissolved Gas (CH_4, C_2H_2, and CO) in Transformer Oil: A DFT Study

Junsheng Ding, Yingang Gui and Hua Huang *

College of Engineering and Technology, Southwest University, Chongqing 400715, China; dingjunshengswu@outlook.com (J.D.); guiyingang@outlook.com (Y.G.)
* Correspondence: huahuangswu@outlook.com

Abstract: Based on density functional calculations, the adsorption and gas sensing properties of transition metal Pt(1-3)-modified $TiSe_2$ for dissolved gas (CH_4, C_2H_2, CO) in transformer oil were studied in this paper. Firstly, the stable structures, density of states, and energy bands of Pt(1-3)-modified $TiSe_2$ were calculated. Then, the structure parameters, density of states, electrostatic potential distribution, and desorption time of Pt(1-3)-modified $TiSe_2$ after adsorbing CH_4, C_2H_2, and CO gas were calculated. The results show that the large binding energy between the transition metal Pt(1-3) modification and the $TiSe_2$ substrate indicates that the modification systems have good structural stability. On the one hand, Pt(1-3) modification improves the conductivity of $TiSe_2$. On the other hand, the transition metal Pt(1-3), which acts as the active site for gas adsorption, obviously enhances the gas adsorption effect, resulting in the significant charge transfer and a change in material conductivity. In summary, Pt(1-3)-modified $TiSe_2$ significantly improves the adsorption and gas sensing performance of gas sensing materials for CH_4, C_2H_2, and CO, which provides a new idea for the study of gas sensing materials for online monitoring of transformer working conditions.

Keywords: DFT; dissolved gas detection; Pt modification; $TiSe_2$; adsorption and sensing

Academic Editor:
Celia García-Hernandez

Received: 5 March 2025
Revised: 18 April 2025
Accepted: 21 April 2025
Published: 23 April 2025

Citation: Ding, J.; Gui, Y.; Huang, H. Adsorption and Sensing Performance of Pt(1-3)-Modified $TiSe_2$ for Dissolved Gas (CH_4, C_2H_2, and CO) in Transformer Oil: A DFT Study. *Int. J. Mol. Sci.* **2025**, *26*, 3985. https://doi.org/10.3390/ijms26093985

1. Introduction

An electric power transformer plays a key role in maintaining the stability of the power system, which boosts the voltage to reduce energy loss during power transmission, and maintains voltage stability and active power balance in power distribution. However, the insulation oil and paper inside the transformer inevitably decompose to produce gas at high temperatures during long-term operation, which seriously affects the insulation [1–3]. It may even cause paralysis of the power system. Insulating paper is easily oxidized to produce CO at 120–130 °C during long-time working [4–6]. CH_4 in insulating oil is mainly produced by partial discharge at 200 °C to 300 °C [5,7]; the internal arc discharge above 700 °C mainly produces C_2H_2 [5,8]. Commonly, the fault can be diagnosed by detecting the generated gas. At present, dissolved gas analysis (DGA) is mainly used for this type of transformer fault [9–11]. However, the DGA diagnosis method for transformers with different voltage levels has some problems, such as different standards, high detection cost, and low sensor sensitivity [12]. In this paper, gas sensing materials are constructed based on first-principles calculation [13,14], and the adsorption performance and gas sensing performance of the gas sensor for dissolved gas in transformer oil were analyzed, which

provides ideas for the design of new gas sensors, and ensures the security and stable operation of the transformer.

Two-dimensional materials are commonly used as gas sensing materials [15,16]; they have the advantages of high specific surface area, sensitive electronic characteristics to environmental changes, strong surface activity, and atomic thickness [17,18]. In addition, transition metal modification on two-dimensional materials can further enhance the adsorption and gas sensing performance for gas molecules. Tang found that graphene shows higher adsorption energy, lower desorption temperatures, and better sensitivity for gas molecules after iron and manganese modifications [19]. Liu found that Ir-modified MoS_2 was highly sensitive to the decomposition products of SF_6, especially H_2S [20]. A large number of studies have proved that doping or modifying transition metal atoms on the basis of two-dimensional materials can significantly enhance the adsorption effect. Pt atoms are commonly used in the field of gas sensing due to their good physical and chemical stability [21–24]. Compared with graphene and MoS_2, the conductivity and electronic properties of single-layer $TiSe_2$ are affected by the phase transition of charge density wave, and the energy gap can be completely closed after metal doping [25]. Xiao reported Cu-modified $TiSe_2$ shows a good adsorption effect on CO [26]. Moreover, $TiSe_2$ is a semimetal material with a smaller band gap than a common semiconductor [27–29].

However, few existing studies reported the application of Pt-modified $TiSe_2$ in dissolved gas detection. Based on density functional theory (DFT), this study proposed one to three Pt atoms modified $TiSe_2$ materials (abbreviated as Pt(1-3)-modified $TiSe_2$) for the typical dissolved gases sensing: CH_4, C_2H_2, and CO. By analyzing the band gaps, density of states, electrostatic potential, adsorption energy, adsorption distance, charge transfer, and desorption time, the adsorption effect and sensing performance were analyzed.

2. Results and Discussion

2.1. The Structure of the System and the Optimal Metal Modification Sites

The optimized structures of the intrinsic $TiSe_2$ substrate and dissolved gas molecules (CH_4, C_2H_2, and CO) are shown in Figure 1. CH_4 is a tetrahedral structure centered on the C atom, in which the C-H bond length is 1.097 Å, and the C-H-C bond angle is 109.387°. The H-C-C bond angle of C_2H_2 is 179.713°, and both of C_2H_2 and CO have a linear molecular structure with three bonds as the skeleton, the bond length of the C-C triple bond is 1.211 Å, which is greater than that of the C-O triple bond 1.142 Å, indicating that the carbon atoms of the latter are subjected to greater interatomic forces. The C-H bond of C_2H_2 is 1.071 Å, which is slightly smaller than that of CH_4, indicating that the binding effect of C_2H_2 on H atom is greater than that of CH_4 after structural optimization; the Ti-Se bond length is 2.57 Å, which is close to the bond length of 2.9 Å measured in previous studies [30], which verified the reliability of the calculation results.

The results show that the top and hollow sites of metal atoms on $TiSe_2$ have better mechanical and electronic properties [31,32]. As shown in Figure 2a, there are five potential modification positions of Pt(1-3) on $TiSe_2$: top of the Ti atoms (P1 position), top of the Se atoms (P2 position), between two Ti atoms (P3 position), above the equilateral triangle formed by the top three Ti atoms (P4 position), between two adjacent Ti atoms in the same top layer (P5 position). Among these modification positions, the system with the largest metal modification binding energy was used as a gas-sensitive material for gas adsorption. The results show that the maximum E_b of single Pt modification (Pt1-$TiSe_2$) is −4.4059 eV by P4. The maximum E_b of double Pt modification (Pt2-$TiSe_2$) is −6.4344 eV by two adjacent P2 positions. The maximum E_b of triple Pt modification (Pt3-$TiSe_2$) is −7.2988 eV by two Pt at P1 and P2 positions, and another Pt connected to the two Pt. The most stable modification positions after geometric optimization are shown in Figure 2b–d.

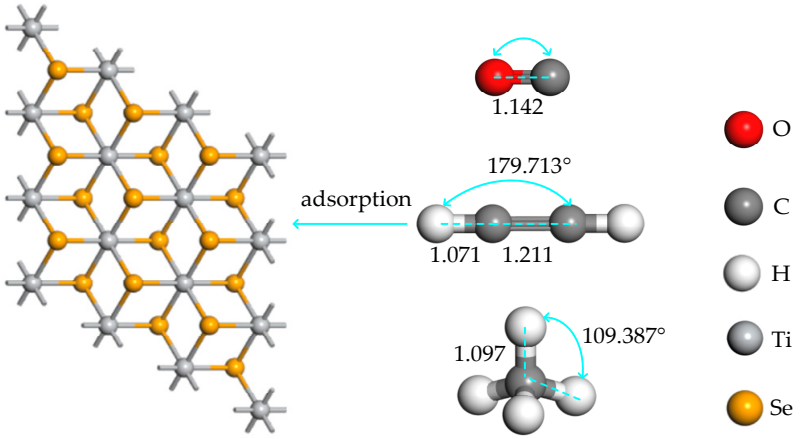

Figure 1. The molecular structure of the $TiSe_2$ substrate and adsorbed gas, and the unit of adsorption distance is Å.

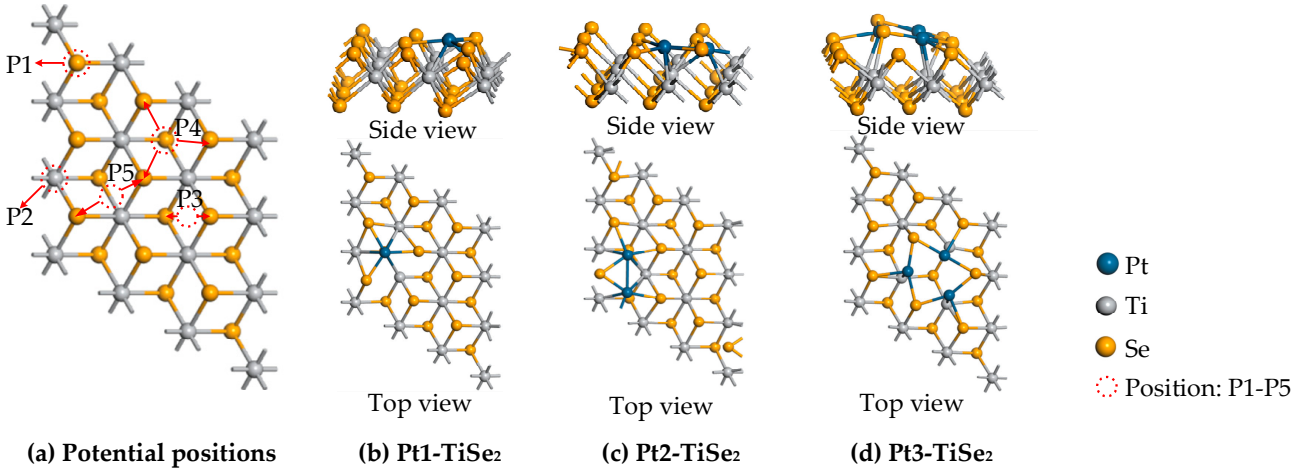

Figure 2. (**a**) Potential modification points and (**b**–**d**) the most stable structure of Pt(1-3)-modified $TiSe_2$.

The density of states of intrinsic $TiSe_2$ and the most stable Pt(1-3)-modified $TiSe_2$ were analyzed to further explore the effect of Pt modification on the electronic properties of the $TiSe_2$ system. As shown in Figure 3a, the black curve represents the density of states of the intrinsic $TiSe_2$ before modification, and the red, blue, and green curves represent the density of states after modification of 1 to 3 Pt atoms, respectively. The results show that higher curves around the Fermi level 0 eV indicate enhanced electron transitions and increased conductivity. In addition, the curve moves to the left toward the lower energy, indicating that stability improves after the modification. The degree of leftward motion of the density of states near the Fermi level is Pt3-$TiSe_2$ > Pt2-$TiSe_2$ > Pt1-$TiSe_2$, which is consistent with the magnitude of binding energy. The energy bands of Pt(1-3)-modified $TiSe_2$ were shown in Figure 3b–d, the modified energy gap is only about 0.01 eV, and the electrons can easily transfer to the conduction band. The energy band near and above 0 eV is more dense, providing more positions for the electron transition. As a result, Pt atom modification increases the electron transition probability and material conductivity.

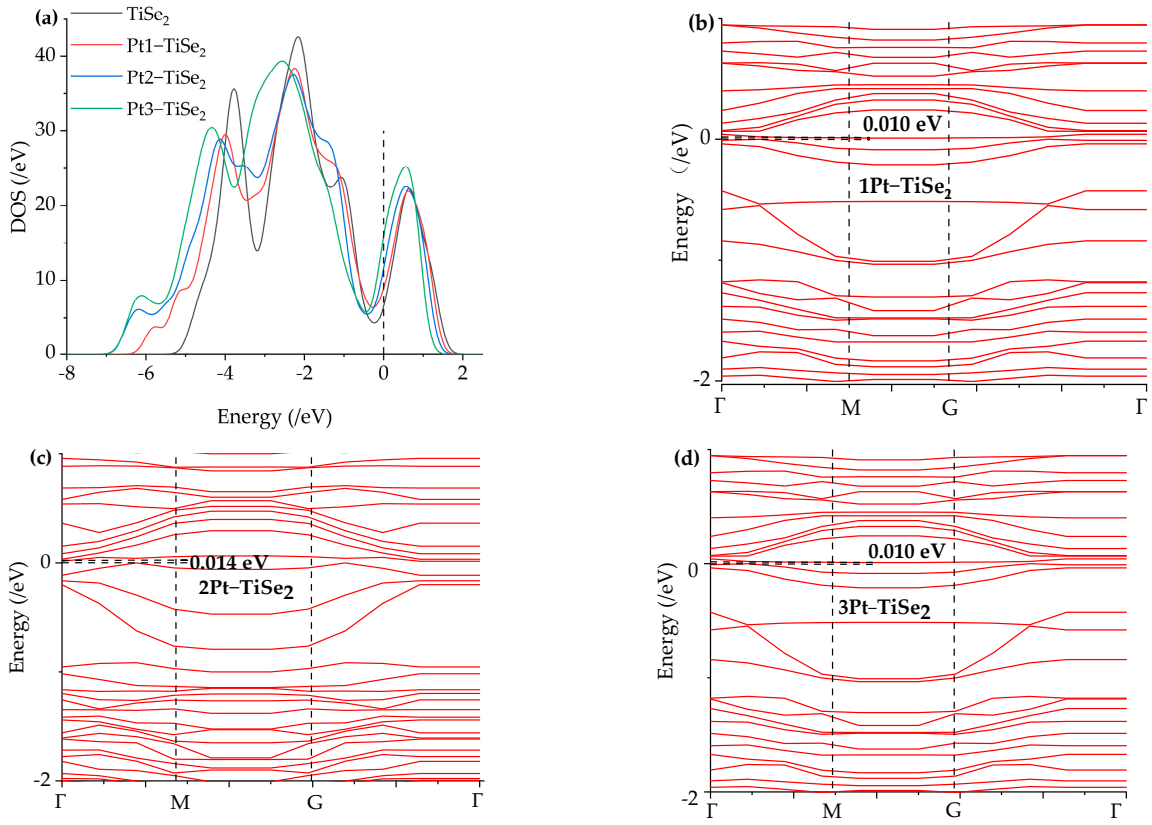

Figure 3. (**a**) density of states of Pt(1-3)-modified $TiSe_2$ and $TiSe_2$, (**b**–**d**) energy band of Pt(1-3)-modified $TiSe_2$.

2.2. Gas Adsorption Property Analysis

2.2.1. CH_4 Gas Adsorption

The CH_4 adsorption calculation was performed based on the most stable Pt(1-3)-modified $TiSe_2$. Due to the different spatial relative positions of gas molecules and Pt(1-3)-modified $TiSe_2$, the adsorption energy, charge transfer, and adsorption distance of the most stable Pt(1-3)-modified $TiSe_2$ are shown in Table 1. The most stable adsorption structures of intrinsic $TiSe_2$ and Pt(1-3)-modified $TiSe_2$ for CH_4 are shown in Figure 4. Table 1 shows that the maximum adsorption energy of $CH_4/TiSe_2$ system is −0.297 eV, and the maximum adsorption energy of CH_4/Pt(1-3)-modified $TiSe_2$ systems are −0.250 eV, −0.248 eV, and −0.270 eV, respectively, indicating there are few changes in the adsorption energy of CH_4 before and after modification. However, the adsorption distance between $CH_4/TiSe_2$ and CH_4/Pt(1-3)-modified $TiSe_2$ system decreased from 3.416 Å to 2.852 Å, 3.303 Å, and 3.112 Å, respectively. The interaction between the gas molecules and the substrate was stronger after modification, which can also be confirmed by the charge transfer. The CH_4 charge transfer before and after modification is −0.054 e, −0.062 e, −0.060 e, and −0.061 e, respectively. CH_4 receives electrons during adsorption and obtains more electrons through the transfer with the modified Pt atoms. Besides, the charge transfer of the metal before and after adsorption is also analyzed; the electrons lost by Pt are 0.028 e, 0.043 e, and 0.052 e. According to the charge transfer of CH_4 and Pt atoms, the electron transfer is most active upon 3 Pt modification, which also corresponds to the large adsorption energy (−0.270 eV) and small adsorption distance (3.112 Å).

Table 1. Adsorption parameters of the intrinsic $TiSe_2$ and Pt(1-3)-modified $TiSe_2$ for CH_4 gas.

System	E_{ads} (eV)	Q_t (e)	Distance (Å)
$CH_4/TiSe_2$	−0.297	−0.054	3.416
$CH_4/Pt1\text{-}TiSe_2$	−0.250	−0.062	2.852
$CH_4/Pt2\text{-}TiSe_2$	−0.248	−0.060	3.303
$CH_4/Pt3\text{-}TiSe_2$	−0.270	−0.061	3.112

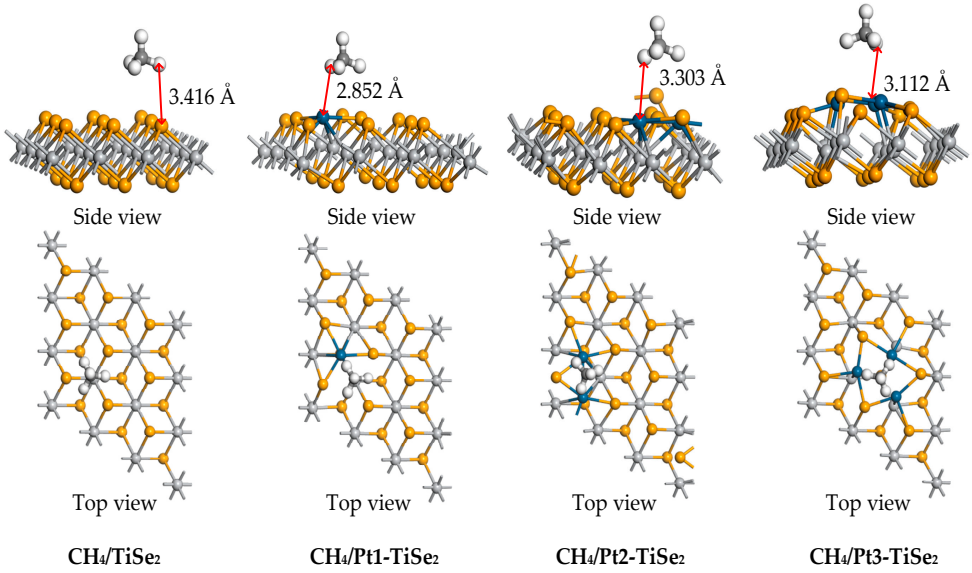

Figure 4. The stable structure of intrinsic $TiSe_2$ and Pt(1-3)-modified $TiSe_2$ for adsorbing CH_4 gas.

The total density of states (TDOS), partial density of states (PDOS), and electrostatic potential (ESP) of the adsorption system are analyzed to further analyze the molecular interactions during the adsorption process, as shown in Figure 5. In Figure 5a, the red, blue, and green curves represent TDOS after modifying 1 to 3 Pt. Compared with the black curve of intrinsic $TiSe_2$, the curve moves up after the 1 to 3 Pt modification near the Fermi level, resulting in an increase in conductivity, which is also consistent with the charge transfer in Table 1. The TDOS of the modified system showed new peaks between −7.5 eV and −5 eV, and the combined PDOS analysis showed that these peaks are due to the modified Pt-d orbital. For PDOS of $CH_4/TiSe_2$ in Figure 5e, the interaction of Se-p, H-s, and C-p orbits is strong between −5 eV and −2.5 eV. The PDOS curves of $CH_4/Pt1\text{-}TiSe_2$ in Figure 5f indicate that there is orbital hybridization between Pt-p, H-s, and C-p. The PDOS of $CH_4/Pt2\text{-}TiSe_2$ in Figure 5g shows an interaction of H-s with Se-p. The PDOS of $CH_4/Pt3\text{-}TiSe_2$ in Figure 5h shows that Pt-d hybridizes with C-p. Figure 5b–d shows the ESP of the $CH_4/Pt(1\text{-}3)$-modified $TiSe_2$ system, and blue to red represents from low to high potential. The results show that the potential around C in CH_4 is lower than the substrate potential, and the potential on the H atom surface is similar to that of the substrate. Also, the substrate and gas potential do not overlap, indicating that the charge transfer during adsorption tends to be between H atoms and the substrate.

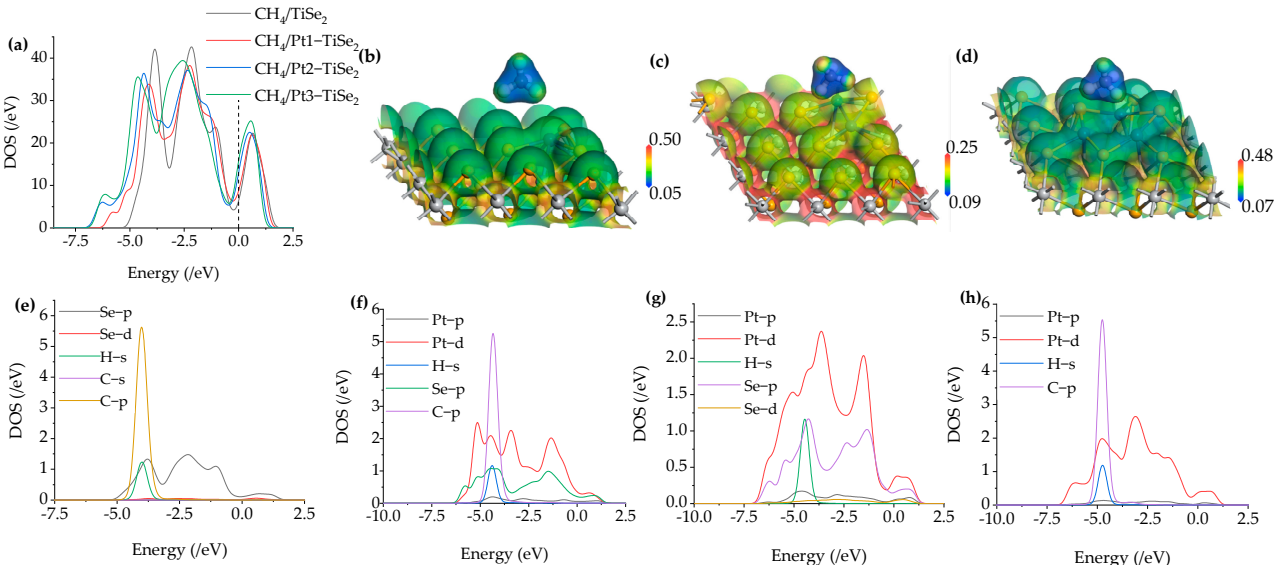

Figure 5. (**a**) The TDOS of $CH_4/TiSe_2$ and CH_4/Pt(1-3)-modified $TiSe_2$, (**b**–**d**) The ESP of CH_4/Pt(1-3)-modified $TiSe_2$, (**e**–**h**) The PDOS of $CH_4/TiSe_2$ and CH_4/Pt(1-3)-modified $TiSe_2$.

2.2.2. C_2H_2 Gas Adsorption

The parameters and structures of the most stable $CH_4/TiSe_2$ and CH_4/Pt(1-3)-modified $TiSe_2$ systems are shown in Table 2 and Figure 6. The maximum adsorption energy of $C_2H_2/TiSe_2$ for C_2H_2 gas is −0.405 eV, and the maximum adsorption energy of C_2H_2/Pt(1-3)-modified $TiSe_2$ is −0.940 eV, −0.489 eV, and −0.422 eV, respectively. Among them, the adsorption energy of C_2H_2 was most significantly improved after one Pt modification. The adsorption distance between the substrate and the gas molecules before and after modifying 1 to 3 Pt decreased from 3.503 Å to 2.194 Å, 2.676 Å, and 3.071 Å, which enhanced the intermolecular force and favored the gas adsorption. The amount of C_2H_2 charge transfer in $C_2H_2/TiSe_2$ and C_2H_2/Pt(1-3)-modified $TiSe_2$ systems is −0.019 e, 0.031 e, 0.053 e, and −0.004 e, respectively. In addition, the electrons lost by Pt were 0.080 e, 0.032 e, and 0.031 e, respectively. Among them, the metal atoms transfer the most electrons after modifying one Pt. Considering the C_2H_2 charge transfer and metal charge transfer, Pt1-$TiSe_2$ has the most active electron transfer during C_2H_2 adsorption, which also corresponds to the shortest adsorption distance of 2.194 Å and the maximum adsorption energy of 0.940 eV. This shows that $TiSe_2$ modified with one Pt can comprehensively improve the adsorption behavior of C_2H_2.

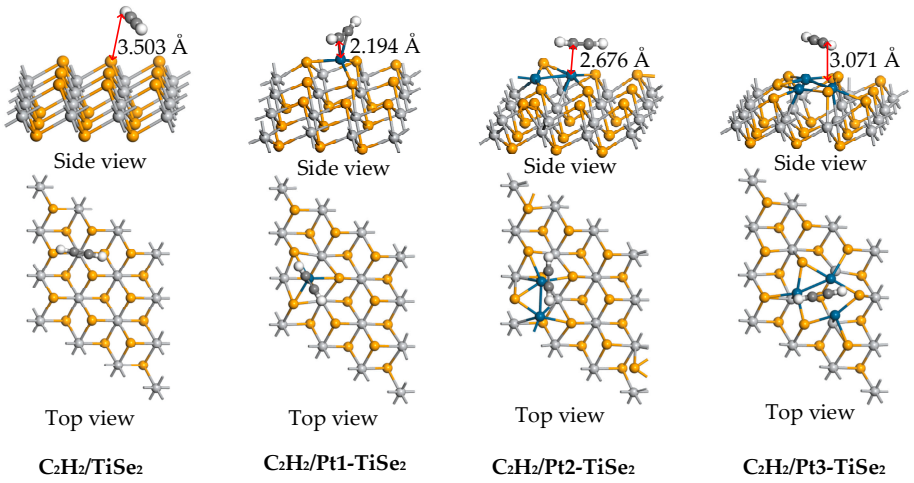

Figure 6. The stable structure of intrinsic $TiSe_2$ and Pt(1-3)-modified $TiSe_2$ for adsorbing C_2H_2 gas.

Table 2. Adsorption parameters of the intrinsic $TiSe_2$ and Pt(1-3)-modified $TiSe_2$ for C_2H_2 gas.

System	E_{ads} (eV)	Q_t (e)	Distance (Å)
$C_2H_2/TiSe_2$	−0.405	−0.019	3.503
C_2H_2/Pt1-$TiSe_2$	−0.940	0.031	2.194
C_2H_2/Pt2-$TiSe_2$	−0.489	0.053	2.676
C_2H_2/Pt3-$TiSe_2$	−0.422	−0.004	3.071

The TDOS and PDOS after C_2H_2 adsorption are shown in Figures 7a and 7e–h, respectively. Figure 7a shows that the TDOS curve of C_2H_2/Pt(1-3)-modified $TiSe_2$ system shifts up at the Fermi level compared with $C_2H_2/TiSe_2$, and the conductivity of the system enhances after Pt modification. Figure 7e–h show that the peaks of the TDOS curve near −5 eV, −2.5 eV are mainly from the contribution of the C-p orbit and the Pt-d orbit. However, the peaks of TDOS in C_2H_2/Pt1-$TiSe_2$ and C_2H_2/Pt2-$TiSe_2$ systems decrease at these two energy levels due to the hybridization of Pt-p orbital and C1-p, C2-p orbitals. Figure 7e shows the hybridization of C-p and H-s orbitals near −7.5 eV, and the interaction of Se-p, Se-d, and C-p orbitals appears near 0 eV. In addition, a new peak appeared between −7.5 eV and −5 eV after Pt modification, according to the corresponding energy level in PDOS, Figure 7f shows that the reason is the hybridization between the p orbitals of the two C atoms and Pt-d orbital after adsorption, Figure 7g shows that reason is the highest Pt-d orbital, and Figure 7h shows that the reason is the hybridization between the Se-p and Pt-d orbitals.

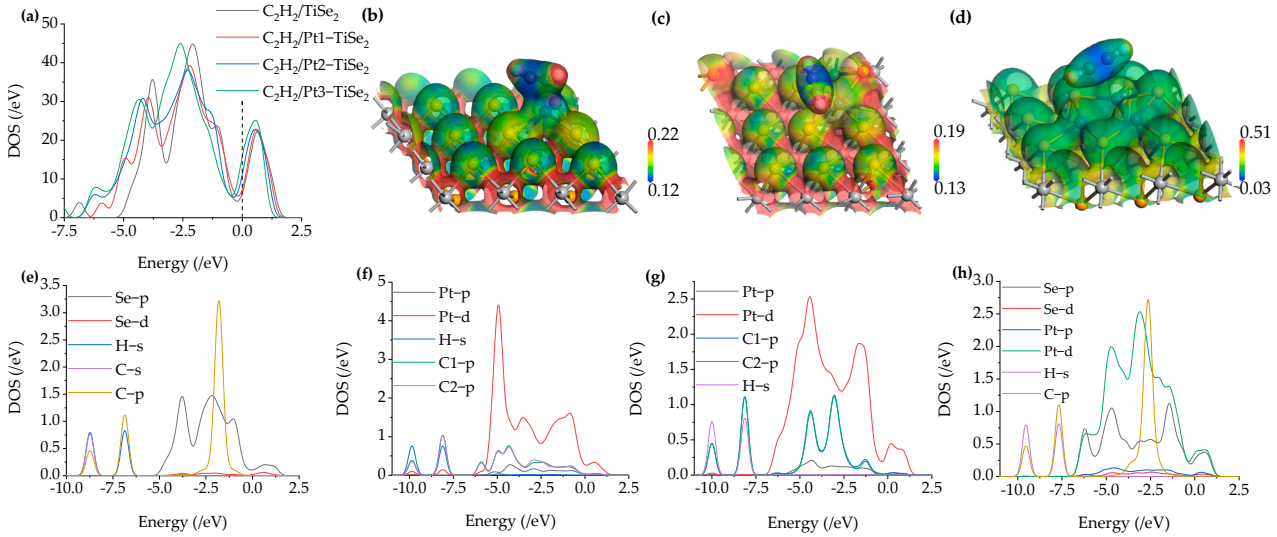

Figure 7. (**a**) The TDOS of $C_2H_2/TiSe_2$ and C_2H_2/Pt(1-3)-modified $TiSe_2$, (**b**–**d**) The ESP of C_2H_2/Pt(1-3)-modified $TiSe_2$, (**e**–**h**) The PDOS of $C_2H_2/TiSe_2$ and C_2H_2/Pt(1-3)-modified $TiSe_2$.

The ESP of the C_2H_2/Pt(1-3)-modified $TiSe_2$ system is shown in Figure 7b–d, respectively, where the color of blue to red indicates the potential from low to high. The results show that the potential on the H surface is higher than that around C. The potential distribution around the two C atoms in the C_2H_2 molecules of the C_2H_2/Pt1-$TiSe_2$ and C_2H_2/Pt2-$TiSe_2$ systems is not identical, but the potential of the C atoms is basically the same in the C_2H_2/Pt3-$TiSe_2$ system. The red color on the H atom surface is lighter than the former two, indicating that the potential is lower. Additionally, Figure 7b shows that the potential distribution of C_2H_2 after adsorption overlaps with that of a modified Pt, which indicates that the gas and substrate are more active in the adsorption process, and the electron transfer is easier. In addition, the blue color above the overlap is darker than the blue color below, indicating a lower upper potential, and the electron moves from a lower potential to a higher potential. Thus, the gas

loses electrons, which is consistent with the loss of 0.031 e at the maximum adsorption energy position after one Pt modification in Table 2.

2.2.3. CO Gas Adsorption

The adsorption parameters and adsorption structures of intrinsic $TiSe_2$ and Pt(1-3)-modified $TiSe_2$ for CO gas at the maximum adsorption energy are shown in Table 3 and Figure 8. The maximum adsorption energy of the CO/$TiSe_2$ system and the CO/Pt(1-3)-modified $TiSe_2$ system changed from −0.219 eV to −1.338 eV, −0.851 eV, and −0.703 eV, respectively, which significantly improved the adsorption energy, especially after one Pt was modified. Correspondingly, the adsorption distance decreased from 3.594 Å to 1.910 Å, 1.946 Å, and 1.986 Å, respectively. The amount of CO charge transfer before and after modification was −0.002 e, 0.001 e, 0.001 e, and 0.004 e, which shows that the amount of CO charge transfer was very small. In addition, the metal atoms lost electrons during the adsorption process, and the charge transfer amounts were 0.034 e, 0.003 e, and 0.001 e, respectively, indicating that one Pt modification lost many more electrons. Therefore, by combining the charge transfer of CO and Pt, it is found that the charge transfer is the most active after modifying one Pt, which is consistent with the shortest adsorption distance of 1.910 Å and the maximum adsorption energy of −1.338 eV.

Table 3. Adsorption parameters of the intrinsic $TiSe_2$ and Pt(1-3)-modified $TiSe_2$ for CO gas.

System	E_{ads} (eV)	Q_t (e)	Distance (Å)
CO/$TiSe_2$	−0.219	−0.002	3.594
CO/Pt1-$TiSe_2$	−1.338	0.001	1.910
CO/Pt2-$TiSe_2$	−0.851	0.001	1.946
CO/Pt3-$TiSe_2$	−0.703	0.004	1.986

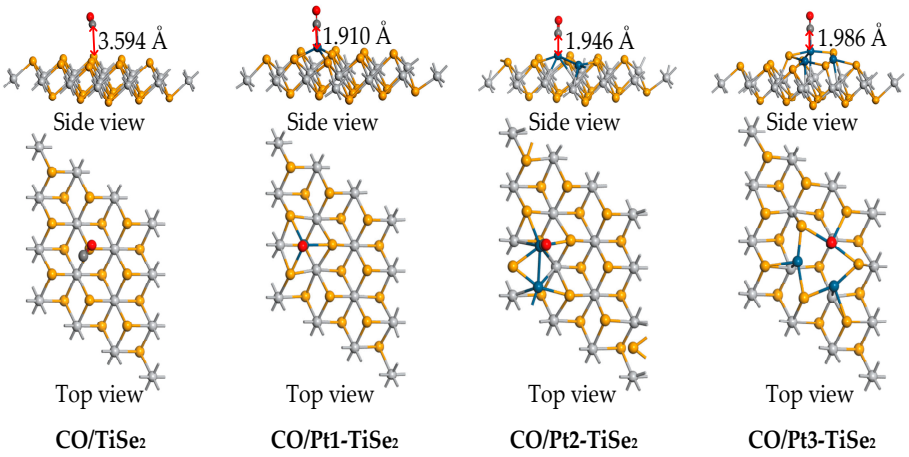

Figure 8. The stable structure of intrinsic $TiSe_2$ and Pt(1-3)-modified $TiSe_2$ for adsorbing CO gas.

TDOS and PDOS after CO adsorption are shown in Figures 9a and 9e–h, respectively. The green curve in Figure 9a corresponds to the TDOS curve of the intrinsic $TiSe_2$ after CO adsorption, while the black, red, and blue curves correspond to the TDOS curve of CO adsorption after 1 to 3 Pt-modified $TiSe_2$, respectively. Figure 9a shows that the black, red, and blue curves near the Fermi level 0 eV are slightly higher than the green curves, indicating that the conductivity enhances during the adsorption process after modifying Pt. According to the PDOS curve in Figure 9e–h, it is found that the Pt-d and Se-p orbits coincide at 0 eV, and the Pt-p, Se-d, C-p, and O-P orbits also coincide at 0 eV, indicating that electrons are shared to enhance conductivity. Figure 9e shows that in the CO/$TiSe_2$ system, C-p is hybridized with Se-p orbits between −5 eV and −2.5 eV. Furthermore, peaks were

observed in the TDOS curve near −2.5 eV and −4 eV, which were mainly contributed by Se-p and Pt-d orbitals, according to the PDOS. However, the two peaks of the TDOS curve of CO/Pt(1-3)-modified $TiSe_2$ are decreased at these two energy levels. Figure 9f–h show that the decrease may possibly be caused by the hybridization between the Se-d and the O-p orbit near −2.5 eV, and the hybridization between Pt-p and O-p near −4 eV. It is also found that the TDOS curves of CO/Pt(1-3)-modified $TiSe_2$ showed new peaks at −7.5 eV and 10 eV compared with that of CO/$TiSe_2$, and the PDOS curve found that it was mainly caused by Pt-d, C-p, and O-p orbitals.

The ESP of the most stable CO/Pt(1-3)-modified $TiSe_2$ systems is shown in Figure 9b–d. Compared with the adsorption of CH_4 and C_2H_2, the potential distribution of the gas and substrate upon CO adsorption has overlap after 1-3 pt modifications, which indicates that there is a more active role of electrons between CO and substrate in the adsorption process, which is consistent with the shorter adsorption distance of CO than CH_4 and C_2H_2. Similarly, the overlap of C and Pt(1-3)-modified TiSe2 is observed; the upper site is yellow, and the bottom is green, indicating that the upper site has a higher potential. Thus, the metal loses electrons due to the movement direction of electrons from low to high potential. By comparison, the color span of the overlapping parts in Figure 9b–d is smaller than Figure 7b, indicating smaller potential difference and weaker electron movement, so compared to the C_2H_2/Pt1-modified $TiSe_2$ shown in Figure 7b where the metal loses 0.080 e, the metal in CO/Pt(1-3)-modified $TiSe_2$ loses fewer electrons. Moreover, the blue color on the surface of O in the CO molecule is deeper, indicating that its potential is lower than that of the C atom and the substrate. During the adsorption process, the electrons of O move from the gas molecule to Pt(1-3)-modified $TiSe_2$, which is consistent with the loss of electrons when the adsorption energy of CO is maximum after 1-3 Pt modifications in Table 3.

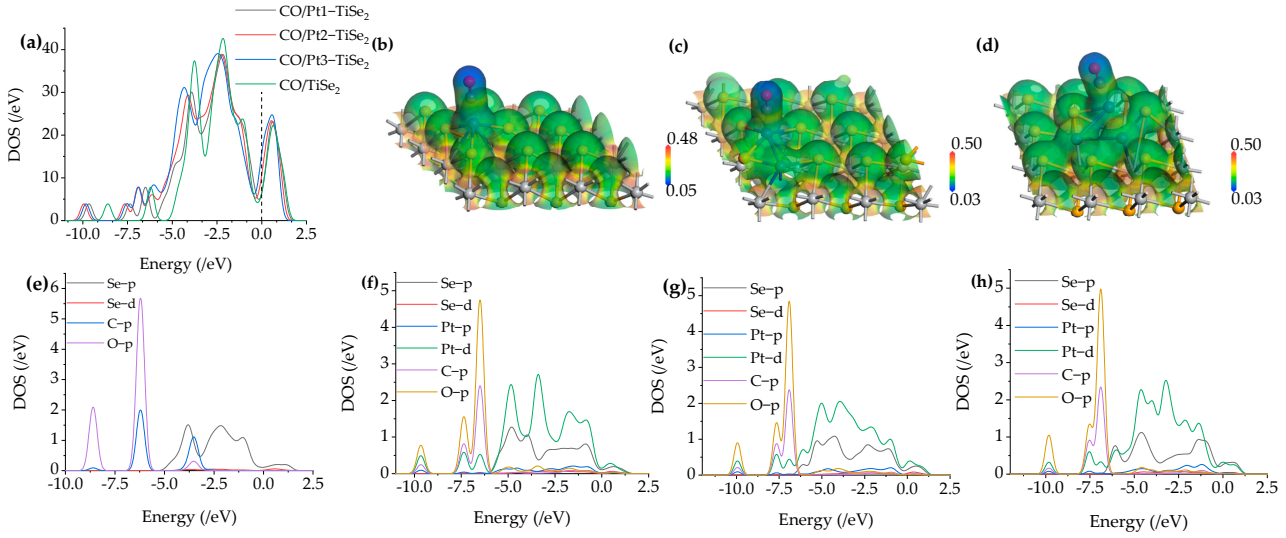

Figure 9. (**a**) The TDOS of CO/TiSe2 and CO/Pt(1-3)-modified $TiSe_2$, (**b**–**d**) The ESP of CO/Pt(1-3)-modified $TiSe_2$, (**e**–**h**) The PDOS of CO/$TiSe_2$ and CO/Pt(1-3)-modified $TiSe_2$.

2.3. Gas Desorption Property Analysis

Pt(1-3)-modified $TiSe_2$-based materials should not only show moderate adsorption capacity to dissolved gas molecules, but the gas should exhibit good desorption ability to ensure the reusability of Pt(1-3)-modified $TiSe_2$-based materials. For CH_4, C_2H_2 and CO, the desorption time was calculated by using the adsorption energy of the most stable adsorption structure of Pt(1-3)-modified $TiSe_2$ for dissolved gas in oil at 298 K, 398 K, and 498 K, to evaluate the reusability of gas sensitive materials, as shown in Figure 10. From Equation (3), the higher the temperature, the shorter the desorption time; the greater

the absolute value of adsorption energy, the longer the desorption time. Therefore, the desorption time increases for a large adsorption energy system at room temperature. An equilibrious desorption time can be reached when the temperature rises, then a good gas sensing response/recovery can be achieved in this temperature range. In Figure 10, the adsorption energy of CH_4 is very small, but the desorption time at the minimum temperature is still minimal, so the system is not the best choice to detect CH_4. For C_2H_2 and CO, it has a large adsorption energy, but the desorption time decreases to 0.8 s and 34 s when the temperature increases to 398 K and 498 K, respectively. Therefore, the Pt(1-3)-modified $TiSe_2$-based gas-sensitive material has good response/recovery performance for C_2H_2 and CO gas.

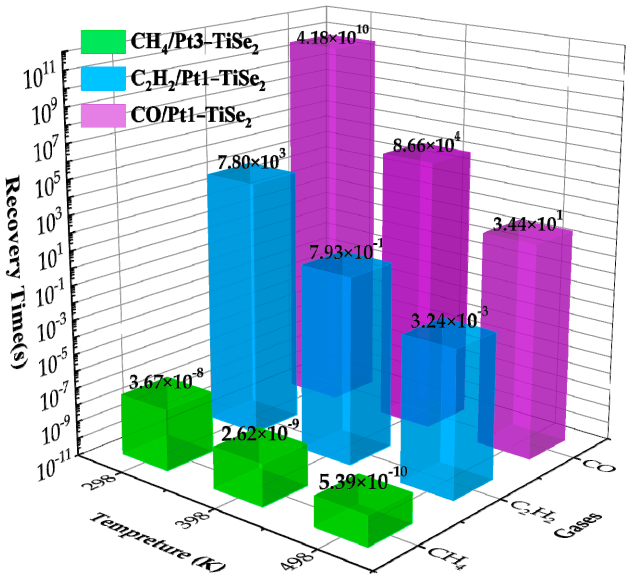

Figure 10. The desorption time of CH_4, C_2H_2, and CO/Pt(1-3)-modified $TiSe_2$ system with maximum adsorption energy at temperatures of 298 K, 398 K, and 498 K.

3. Calculation Methods

All calculations are performed based on the density functional theory of the DMol^3. $TiSe_2$ adopts a triangular prismatic phase crystal of P3m1 space group with a structural shape of Se-Ti-Se triple layers [33,34]. The $TiSe_2$ supercell was built by $3 \times 3 \times 1$ primitive cells along the (0 0 1) direction, and the vacuum layer was set to 20 Å to prevent adjacent $TiSe_2$ layers from interacting in the z direction. Structure optimization is used to obtain the most stable structure of the system, and the function perdew-burke-ernzerhof (PBE) and generalized gradient approximation (GGA) were selected [35,36]. During the geometry optimization process, the convergence standard of self-consistent field is 1×10^{-5} Ha, the maximum atomic force between atoms is 0.002 Ha/Å, and the maximum atomic displacement is 0.005 Å. The number of sampling points of the Brillouin area is set to $7 \times 7 \times 1$ [37,38].

For Pt(1-3)-modified $TiSe_2$, the metal atoms show different modification positions for each modification mode. By calculating the stable structure of different modification positions, the modification position with the maximum binding energy is used for gas adsorption. The binding energy E_b is calculated by Equation (1). $E_{Metal\text{-}TiSe2}$ represents the total energy of the system after the Pt(1-3) metal modification, E_{TiSe2} represents the energy of the intrinsic $TiSe_2$, and E_{Metal} represents the energy of the metal atoms. Due to the different adsorption positions between dissolved gas molecules and Pt(1-3)-modified $TiSe_2$, the adsorption energy (E_{ads}), adsorption distance, and charge transfer (Q_t) are calculated to select the most stable adsorption structures. The adsorption energy E_{ads} is calculated by Equation (2). $E_{gas/metal\text{-}TiSe2}$ represents the total energy after gas adsorption on Pt(1-3)-

modified $TiSe_2$, E_{gas} represents the total energy of the gas molecule, and $E_{Metal\text{-}TiSe2\text{-}max}$ represents the total energy of Pt(1-3)-modified $TiSe_2$. The recovery time is calculated by Equation (3), which represents the time required for the gas response to recover from 100% to 10%. ω represents the trial frequency, which represents the number of times per second that molecules attempt to desorb from the adsorption sites on the surface, typically valued at 10^{12} s^{-1} for solid surfaces. T is Kelvin temperature, and K_B is Boltzmann constant (8.62×10^{-5} eV/K) [39–42].

$$E_b = E_{Metal-TiSe_2} - E_{TiSe_2} - E_{Metal}, \quad (1)$$

$$E_{ads} = E_{gas/Metal-TiSe_2} - E_{gas} - E_{Metal-TiSe_2-\max}, \quad (2)$$

$$\tau = \omega^{-1} \cdot \exp(-E_{ads}/TK_B) \quad (3)$$

4. Conclusions

Based on DFT calculations, the behavior of intrinsic $TiSe_2$ and Pt(1-3)-modified $TiSe_2$ adsorption to CO, CH_4, and C_2H_2 was investigated. Firstly, the structures of intrinsic $TiSe_2$, Pt(1-3)-modified $TiSe_2$, dissolved gases, and gas adsorption were constructed. Then, the gas adsorption and sensing properties of gases on intrinsic $TiSe_2$ and Pt(1-3)-modified $TiSe_2$ are studied by analyzing the adsorption TDOS, PDOS, ESP, and desorption time. In summary, Pt(1-3) atoms form stable binding structures on the $TiSe_2$ surface with binding energy in the order of Pt3-$TiSe_2$ > Pt2-$TiSe_2$ > Pt1-$TiSe_2$. The energy band gaps of the Pt(1-3)-modified $TiSe_2$ system are about zero, and the energy band of the conduction band around the Fermi level becomes denser. The DOS of Pt(1-3)-modified $TiSe_2$ systems increases and moves left near the Fermi level. As a result, Pt(1-3) atom modification increases the conductivity of $TiSe_2$. Pt(1-3) atom modification increases the adsorption capability of $TiSe_2$ to CO, CH_4, and C_2H_2. Particularly, Pt1-$TiSe_2$ has the maximum adsorption energy for CO (−1.338 eV) and C_2H_2 (−0.940 eV). However, Pt(1-3)-modified $TiSe_2$ shows weak adsorption capacity to CH_4. Combining with the TDOS, PDOS, and ESP analysis, the conductivity of the adsorption systems significantly changes during the adsorption of CO, CH_4, and C_2H_2, resulting in good gas sensing properties. In Figure 5a, Figure 7a, and Figure 9a, the TDOS curves after adsorption of the three gas molecules show a significant increase near the Fermi level, indicating a decrease in the sensor's resistance response. This provides theoretical support for the sensor's sufficient sensitivity. The desorption time analysis shows that the desorption time of CH_4 was very small at all temperatures; the desorption time of C_2H_2 is 0.8 s at 398 K, and the desorption time of CO is 34s at 498 K. Overall, Pt1-$TiSe_2$ has good gas response/recovery performance for dissolved gas in transformer oil. The results of this study lay the foundation for the experimental preparation of a gas sensor for online monitoring and fault diagnosis of transformer failure.

Author Contributions: Conceptualization, J.D.; methodology, Y.G.; software, H.H.; validation, J.D.; formal analysis, J.D.; investigation, J.D.; resources, H.H.; data curation, J.D.; writing—original draft preparation, J.D.; writing—review and editing, Y.G.; visualization, Y.G.; supervision, Y.G.; project administration, Y.G. All authors have read and agreed to the published version of the manuscript.

Funding: This research received no external funding.

Institutional Review Board Statement: Not applicable.

Informed Consent Statement: Not applicable.

Data Availability Statement: Data are contained within the article.

Conflicts of Interest: The authors declare no conflicts of interest.

References

1. Mehmood, M.A.; Nazir, M.T.; Li, J.; Wang, F.; Azam, M.M. Comprehensive investigation on service aged power transformer insulating oil after decades of effective performance in field. *Arab. J. Sci. Eng.* **2020**, *45*, 6517–6528. [CrossRef]
2. Phadungthin, R.; Ekkachai, C.; Haema, J.; Suwanasri, T. Analysis of insulating oil to evaluate the condition of power transformer. In Proceedings of the ECTI-CON2010: The 2010 ECTI International Conference on Electrical Engineering/Electronics, Computer, Telecommunications and Information Technology, Chiang Mai, Thailand, 19–21 May 2010; pp. 108–111.
3. Thiviyanathan, V.A.; Ker, P.J.; Leong, Y.S.; Abdullah, F.; Ismail, A.; Jamaludin, M.Z. Power transformer insulation system: A review on the reactions, fault detection, challenges and future prospects. *Alex. Eng. J.* **2022**, *61*, 7697–7713. [CrossRef]
4. Fernández, I.; Delgado, F.; Ortiz, F.; Ortiz, A.; Fernández, C.; Renedo, C.J.; Santisteban, A. Thermal degradation assessment of kraft paper in power transformers insulated with natural esters. *Appl. Therm. Eng.* **2016**, *104*, 129–138. [CrossRef]
5. Golarz, J. Understanding dissolved gas analysis (DGA) techniques and interpretations. In Proceedings of the 2016 IEEE/PES Transmission and Distribution Conference and Exposition (T&D), Dallas, TX, USA, 3–5 May 2016; pp. 1–5.
6. Jalbert, J.; Rodriguez-Celis, E.M.; Arroyo-Fernández, O.H.; Duchesne, S.; Morin, B. Methanol marker for the detection of insulating paper degradation in transformer insulating oil. *Energies* **2019**, *12*, 3969. [CrossRef]
7. Mehta, A.; Sharma, R.N.; Chauhan, S. Partial discharge study by monitoring key gases of power transformers. In Proceedings of the 2011 3rd International Conference on Electronics Computer Technology, Kanyakumari, India, 8–10 April 2011; pp. 183–186.
8. Zhou, S.; Iannuzzi, D. Immersion photoacoustic spectrometer (iPAS) for arcing fault detection in power transformers. *Opt. Lett.* **2019**, *44*, 3741–3744. [CrossRef]
9. Bakar, N.A.; Abu-Siada, A.; Islam, S. A review of dissolved gas analysis measurement and interpretation techniques. *IEEE Electr. Insul. Mag.* **2014**, *30*, 39–49. [CrossRef]
10. Bustamante, S.; Manana, M.; Arroyo, A.; Castro, P.; Laso, A.; Martinez, R. Dissolved gas analysis equipment for online monitoring of transformer oil: A review. *Sensors* **2019**, *19*, 4057. [CrossRef]
11. Duval, M. Dissolved gas analysis: It can save your transformer. *IEEE Electr. Insul. Mag.* **1989**, *5*, 22–27. [CrossRef]
12. Ashkezari, A.D.; Saha, T.K.; Ekanayake, C.; Ma, H. Evaluating the accuracy of different DGA techniques for improving the transformer oil quality interpretation. In Proceedings of the AUPEC 2011, Brisbane, QLD, Australia, 25–28 September 2011; pp. 1–6.
13. Majid, A.; Khadim, B.; Alkhedher, M.; Haider, S.; Akhtar, M.S. Modeling of inert gas sensors using first principles methods. *IEEE Sens. J.* **2023**, *23*, 18118–18124. [CrossRef]
14. Ouyang, B. First-Principles algorithm for air quality electrochemical gas sensors. *ACS Sens.* **2020**, *5*, 2742–2746. [CrossRef]
15. Vargas-Bernal, R. Electrical properties of two-dimensional materials used in gas sensors. *Sensors* **2019**, *19*, 1295. [CrossRef] [PubMed]
16. Liu, X.; Ma, T.; Pinna, N.; Zhang, J. Two-dimensional nanostructured materials for gas sensing. *Adv. Funct. Mater.* **2017**, *27*, 1702168. [CrossRef]
17. Varghese, S.S.; Varghese, S.H.; Swaminathan, S.; Singh, K.K.; Mittal, V. Two-dimensional materials for sensing. *Graphene Beyond* **2015**, *4*, 651–687.
18. Wang, B.; Gu, Y.; Chen, L.; Ji, L.; Zhu, H.; Sun, Q. Gas sensing devices based on two-dimensional materials: A review. *Nanotechnology* **2022**, *33*, 252001. [CrossRef]
19. Tang, H.; Xiang, Y.; Zhan, H.; Zhou, Y.; Kang, J. DFT investigation of transition metal-doped graphene for the adsorption of HCl gas. *Diam. Relat. Mater.* **2023**, *136*, 109995. [CrossRef]
20. Liu, H.; Wang, F.; Hu, K.; Li, T.; Yan, Y.; Li, J. The adsorption and sensing performances of Ir-modified MoS_2 monolayer toward SF_6 decomposition products: A DFT study. *Nanomaterials* **2021**, *11*, 100. [CrossRef]
21. Tan, S.; Bi, M.; Lei, S.; He, X.; Hu, X.; He, J.; Jiang, T. Adsorption of SF_6 decomposition gases (H_2S, SO_2 and SOF_2) on TM (Pd and Pt) modified monolayer ZrS_2: A DFT study. *Comput. Theor. Chem.* **2024**, *1236*, 114586. [CrossRef]
22. Wang, X.; Gui, Y.; Ding, Z.; Xu, H.; Zeng, H.; Chen, X. Density functional theory study of Pd, Pt, and Au modified GeSe for adsorption and sensing of dissolved gases in transformer oil. *Surf. Interfaces* **2022**, *31*, 101994. [CrossRef]
23. Wang, Y.; Gui, Y.; Yang, J.; Jin, G.; Yang, P.; Gao, M.; Huang, H. DFT study of metal (Ag, Au, Pt)-modified SnS_2 for adsorption of SF_6 decomposition gases in gas-insulated switchgear. *Langmuir* **2024**, *40*, 7049–7059. [CrossRef]
24. Shen, J.; Hill, J.M.; Watwe, R.M.; Spiewak, B.E.; Dumesic, J.A. Microcalorimetric, infrared spectroscopic, and DFT studies of ethylene adsorption on Pt/SiO_2 and $Pt{-}Sn/SiO_2$ catalysts. *J. Phys. Chem. B* **1999**, *103*, 3923–3934. [CrossRef]
25. Kolekar, S.; Bonilla, M.; Diaz, H.C.; Hashimoto, M.; Lu, D.; Batzill, M. Controlling the charge density wave transition in monolayer $TiSe_2$: Substrate anddoping effects. *Adv. Quantum Technol.* **2018**, *1*, 1800070. [CrossRef]
26. Xiao, L.; Guo, G.; Zhang, M.; You, M.; Luo, S.; Guo, G.; He, C.; Tang, C.; Zhong, J. Cu- and Al-decorated monolayer $TiSe_2$ for enhanced gas detection sensitivity: A DFT Study. *Langmuir* **2023**, *39*, 18631–18643. [CrossRef] [PubMed]
27. Benesh, G.A.; Woolley, A.M.; Umrigar, C. The pressure dependences of TiS_2 and $TiSe_2$ band structures. *J. Phys. C Solid State Phys.* **1985**, *18*, 1595. [CrossRef]

28. Markov, M.; Rezaei, S.E.; Sadeghi, S.N.; Esfarjani, K.; Zebarjadi, M. Thermoelectric properties of semimetals. *Phys. Rev. Mater.* **2019**, *3*, 095401. [CrossRef]
29. Zhuang, W.; Chen, Z.; Wang, X. Large-area fabrication of 2D layered topological semimetal films and emerging applications. *Adv. Phys. X* **2022**, *7*, 2034529. [CrossRef]
30. Li, P.; Zheng, X.; Yu, H.; Zhao, G.; Shu, J.; Xu, X.; Sun, W.; Dou, S.X. Electrochemical potassium/lithium-ion intercalation into $TiSe_2$: Kinetics and mechanism. *Energy Storage Mater.* **2019**, *16*, 512–518. [CrossRef]
31. Antonio, J.E.; Cervantes, J.M.; Rosas-Huerta, J.L.; Pilo, J.; Carvajal, E.; Escamilla, R. A first-principles investigation on the electronic and mechanical properties of 1T $TiSe_2$ multilayers for energy storage. *J. Electrochem. Soc.* **2021**, *168*, 030531. [CrossRef]
32. Wu, Q.; Chen, Y.; Hao, X.; Zhu, T.; Cao, Y.; Wang, W. Insight into the anchoring effect of two-dimensional TiX_2 (X=S, Se, Te) materials for Lithium-Sulfur batteries: A DFT study. *J. Electrochem. Soc.* **2021**, *168*, 120516. [CrossRef]
33. Das, S. Quantum Oscillations in Two Dimensional Dirac and Weyl Semimetals. Ph.D. Thesis, The Florida State University, Tallahassee, FL, USA, 2016; 100p.
34. Rossnagel, K.; Kipp, L.; Skibowski, M. Charge-density-wave phase transition in 1T-$TiSe_2$: Excitonic insulator versus band-type Jahn-Teller mechanism. *Phys. Rev. B* **2002**, *65*, 235101. [CrossRef]
35. Blöchl, P.E. Projector augmented-wave method. *Phys. Rev. B* **1994**, *50*, 17953–17979. [CrossRef]
36. Haas, P.; Tran, F.; Blaha, P.; Schwarz, K. Construction of an optimal GGA functional for molecules and solids. *Phys. Rev. B* **2011**, *83*, 205117. [CrossRef]
37. Choudhary, K.; Tavazza, F. Convergence and machine learning predictions of Monkhorst-Pack k-points and plane-wave cut-off in high-throughput DFT calculations. *Comput. Mater. Sci.* **2019**, *161*, 300–308. [CrossRef] [PubMed]
38. Monkhorst, H.J.; Pack, J.D. Special points for Brillouin-zone integrations. *Phys. Rev. B* **1976**, *13*, 5188–5192. [CrossRef]
39. Chakraborty, S.; Mandal, I.; Ray, I.; Majumdar, S.; Sen, A.; Maiti, H.S. Improvement of recovery time of nanostructured tin dioxide-based thick film gas sensors through surface modification. *Sens. Actuators B Chem.* **2007**, *127*, 554–558. [CrossRef]
40. D'Arsié, L.; Alijani, V.; Brunelli, S.T.S.; Rigoni, F.; Di Santo, G.; Caputo, M.; Panighel, M.; Freddi, S.; Sangaletti, L.; Goldoni, A. Improved recovery time and sensitivity to H_2 and NH_3 at room temperature with SnO_x vertical nanopillars on ITO. *Sci. Rep.* **2018**, *8*, 10028. [CrossRef]
41. Gui, Y.; Zeng, X.; Hao, J. Adsorption properties of nCu_2O-graphene (n = 1, 2, 3) for SOF_2 and SO_2F_2 gas molecules. *Diam. Relat. Mater.* **2023**, *139*, 110378. [CrossRef]
42. Tao, L.-Q.; Wang, G.; Hou, P.; Liu, J.; Chen, X. Physisorption behaviors of deoxyribonucleic acid nucleobases and base pairs on bismuthene from theoretical insights. *Appl. Surf. Sci.* **2023**, *627*, 157242. [CrossRef]